

Functionalized pentacenes: a combined theoretical, Raman and UV–Vis spectroscopic study

Juan Aragó · Pedro M. Viruela · Enrique Ortí · Reyes Malavé Osuna ·
Víctor Hernández · Juan T. López Navarrete · Christopher R. Swartz ·
John E. Anthony

Received: 28 June 2010/Accepted: 10 September 2010/Published online: 28 September 2010
© Springer-Verlag 2010

Abstract This work presents an analysis of the evolution of the molecular, vibrational and optical properties of a family of functionalized pentacenes. The analysis is performed on the basis of DFT quantum-chemical calculations in combination with spectroscopic techniques (Raman and UV–Vis). Theoretical calculations show that the bond length C–C/C=C alternation along the peripheral oligoenic ribbons increases with electron-releasing dioxolane substituents and diminishes with electron-withdrawing chlorine atoms and cyano groups. The attachment of triisopropylsilyl ethynyl groups increases the complexity of the Raman spectra. The spectra present many intense features of similar intensities in the 1,200–1,600 cm^{−1} range which are described by a combination of C–C/C=C stretching vibrations and in-plane C–H deformations spreading over the whole pentacene backbone. The absorption spectra display absorption bands in three different energy regions of the UV–Vis electromagnetic range. The spectra are dominated

by a strong absorption band measured in the 300–350 nm region, which undergoes a sizeable red-shift with the substitution pattern, and a low-intensity, three-peak band in the 500–700 nm region, which undergoes a blue- or a red-shift depending on the electronic nature of the substituents. TDDFT calculations enable a detailed description of the trends observed in the absorption spectra.

Keywords Raman spectra · Electronic transitions · Pentacenes · Density functional calculations

1 Introduction

Oligoacenes constitute the most promising class of organic semiconductor materials due to their application for (opto)electronic devices such as organic thin-film transistors (OTFTs) and solar cells [1, 2]. The rigid π-conjugated skeleton, free from conformational disorder, and the extension of the π-conjugation over the whole molecule are decisive characteristics leading to unique electronic properties and densely packed solid-state structures. This packing allows for high charge-carrier mobilities. Among oligoacenes, pentacene is likely to be the most studied system. Pentacene has attracted great interest because it has proven to be one of the most effective compounds in OTFTs with charge-carrier mobilities as high as 5.5 cm² V^{−1} s^{−1} [3]. It has been addressed that molecular ordering has a strong influence in the charge transport efficiency; face-to-face π-stacked structures in the solid favor the charge-carrier mobilities due to optimum π-orbital overlap [4]. However, pentacene displays a “herringbone” packing with a combination of edge-to-face and face-to-face molecular interactions. This packing yields limited π-orbital overlap and may make difficult the charge transport.

Published as part of the special issue celebrating theoretical and computational chemistry in Spain.

J. Aragó · P. M. Viruela · E. Ortí (✉)
Instituto de Ciencia Molecular, Universidad de Valencia,
Valencia 46980, Spain
e-mail: enrique.orti@uv.es

R. Malavé Osuna · V. Hernández · J. T. López Navarrete (✉)
Departamento de Química Física, Universidad de Málaga,
Málaga 29071, Spain
e-mail: teodomiro@uma.es

C. R. Swartz · J. E. Anthony
Department of Chemistry, University of Kentucky, Lexington,
KY 40506, USA

In this sense, numerous attempts have been made to increase face-to-face packing and close contacts in pentacene by variations in deposition methods or by substrate modification [5]. A chemical approach is the direct functionalization with trialkylsilyl ethynyl groups at 6,13 positions of pentacene, which allows for an exquisite control over the solid-state arrangement as well as for an enhancement of the stability and solubility [6–8]. Specifically, the triisopropylsilyl ethynyl (TIPSE) groups (see Fig. 1) induce a two-dimensional brickwork arrangement with primarily face-to-face interactions and improve the π -orbital overlap [6]. This two-dimensional packing was found to be optimal for the use in OTFTs with mobilities as high as $1.5 \text{ cm}^2 \text{ V}^{-1} \text{ s}^{-1}$ [9]. The TIPSE groups not only modify the solid-state properties but also change the energy of both the highest occupied molecular orbital (HOMO) and the lowest unoccupied molecular orbital (LUMO). This change affects the charge injection properties and results in lower charge-carrier mobilities compared to unsubstituted pentacene. In an attempt to improve the electronic properties maintaining the high stability of the TIPSE pentacene derivative, new functionalization patterns such as dioxolane, chlorine and cyano groups were incorporated at the end of the pentacene fragment [10, 11]. The introduction of these substituents has a large impact on the electronic and optical properties. Cyclic ether groups induce a blue-shift of the first absorption band and a decrease of the oxidation potential with respect to TIPSE pentacene, whereas electron-withdrawing groups (chlorine and cyano) lead to a slight red-shift of the first absorption band along with an increase of the oxidation potential.

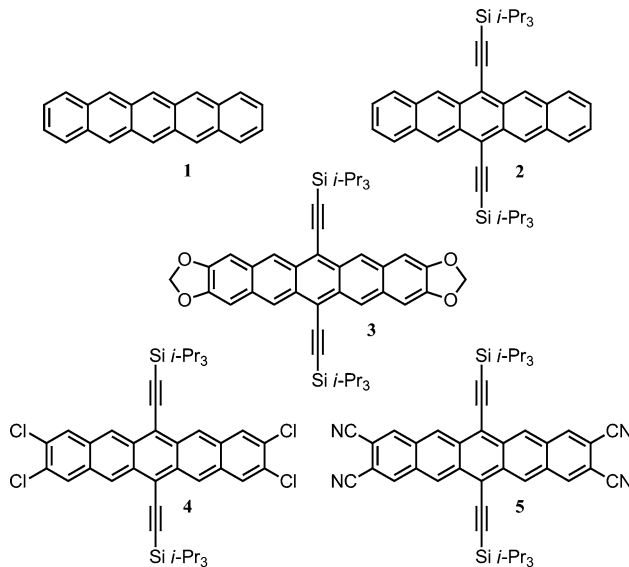


Fig. 1 Chemical structures and labeling of the pentacene derivatives investigated in this work

Quantum-chemical calculations in conjunction with spectroscopic techniques (Raman and UV–Vis) have been proved to be a powerful tool to characterize oligomeric π -conjugated systems [12–17]. In particular, quantum-chemical calculations have been especially useful in rationalizing the structural and electronic properties of oligothiophenes [18–25] and fully fused oligothienoacenes [26–28], the later being closely related to the acene systems discussed here. In this contribution, we perform a joint theoretical and experimental study of a family of functionalized pentacenes (Fig. 1) by means of density functional theory (DFT) and time-dependent DFT (TDDFT) calculations together with spectroscopic techniques (Raman and UV–Vis), with the aim of establishing precise structure–property relationships. The study mainly focuses on analyzing the role of the substitution pattern on the molecular, vibrational and optical properties.

2 Computational and experimental details

DFT calculations were carried out by means of the Gaussian 03 program [29]. All the calculations including geometry optimizations of the ground state, electronic excitation energies and vibrational spectra were performed on the isolated systems using the Becke's three-parameter B3LYP exchange-functional [30, 31]. The 6-31G** basis set [32] was chosen as a compromise between accuracy and applicability to large molecules. Appropriate symmetry constraints for substituted (C_{2h}) and unsubstituted (D_{2h}) pentacenes were imposed.

On the resulting ground-state optimized geometries, harmonic vibrational frequencies and Raman intensities were calculated. We used the often-practiced adjustment of the theoretical force fields in which calculated harmonic vibrational frequencies are uniformly scaled down by a factor of 0.96 for the B3LYP/6-31G** calculations [33–35]. This scaling procedure is often accurate enough to disentangle serious experimental misassignments. All quoted vibrational frequencies reported along the paper are thus scaled values. The theoretical Raman spectra were obtained by convoluting the scaled frequencies with Gaussian functions (10 cm^{-1} width at the half-height). The relative heights of the Gaussians were determined from the theoretical Raman scattering activities.

Vertical electronic transition energies were computed for the twenty lowest-energy electronic excited states using the TDDFT approach [36–38]. This approach has been widely used to study the electronic spectra of large π -conjugated systems such as polyenes [39], polycyclic aromatic hydrocarbons [40–45], fullerenes [46], oligomers of α -oligothiophenes, para-phenylenes and para-phenylenevinylanes [12, 47, 48] and porphyrin-type macrocycles and

oligomers [49–52]. Standard hybrid functionals such as B3LYP have been shown to provide excitation energies that are roughly within 0.3 eV of the experimental data. Despite these encouraging results, the TDDFT approach should be used with caution, because the excitation energies can be affected by quite different errors. Overestimations/underestimations in the 0.4–0.7 eV range are not uncommon, and they can lead to wrong assignments when trying to provide a full interpretation of the electronic spectrum [53]. Molecular orbitals were plotted using Molekel 4.3 [54].

Synthesis and purification of the substituted pentacenes are described elsewhere [6, 7, 11]. UV–Vis–NIR absorption spectra were recorded at room temperature by means of an Agilent 8453 instrument equipped with a diode array for fast recording of all electromagnetic absorptions in the 190- to 1,100-nm spectral region. FT-Raman scattering spectra were collected on a Bruker FRA106/S apparatus equipped with a Nd:YAG laser source ($\lambda_{\text{exc}} = 1,064 \text{ nm}$), in a back-scattering configuration. The operating power for the exciting laser radiation was kept to 100 mW in all the experiments. Samples were analyzed as pure solids in sealed capillaries. Typically, 1,000 scans with 2 cm^{-1} spectral resolution were averaged to optimize the signal-to-noise ratio.

3 Results and discussion

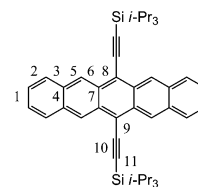
3.1 Molecular structure

To investigate the effect of substituents on the molecular structure of pentacene, geometry optimizations of compounds **1–5** were systematically performed at the B3LYP/6-31G** level. Table 1 collects the optimized bond lengths computed for pentacenes **1–5** as well as the X-ray data reported for **2** [6]. Pentacenes can be visualized as two parallel oligoenic ribbons linked by single C–C bonds rather than a chain of fused aromatic benzene rings [55]. For all the five pentacenes **1–5**, the bond length alternation between single and double C–C/C=C bonds along each oligoenic ribbon progressively diminishes on going from the outer to central rings indicating an efficient electron delocalization along the periphery of the π -conjugated backbone. In contrast, the inner single C–C bonds joining the two parallel oligoenic ribbons hardly change (see Table 1).

As can be seen from Table 1, the attachment of TIPSE groups to the central benzene ring has a soft impact on the carbon skeleton and mainly affects the carbon–carbon (CC) bond lengths of the central benzene ring to which they are attached. Bond 8 undergoes a noticeable lengthening, passing from 1.402 Å in **1** to 1.425 Å in **2**, whereas bond 7

Table 1 B3LYP/6-31G**-optimized bond lengths (Å) calculated for compounds **1–5**. X-ray data from Ref. [6] are included within parentheses for compound **2**

Bond number	1	2	3	4	5
<i>Pentacene</i>					
1	1.433	1.432 (1.427)	1.427	1.441	1.453
2	1.365	1.366 (1.350)	1.356	1.366	1.373
3	1.436	1.434 (1.436)	1.442	1.431	1.429
4	1.455	1.449 (1.440)	1.457	1.446	1.448
5	1.389	1.390 (1.384)	1.388	1.390	1.390
6	1.415	1.411 (1.407)	1.413	1.411	1.411
7	1.457	1.451 (1.444)	1.448	1.451	1.451
8	1.402	1.425 (1.419)	1.424	1.425	1.425
<i>TIPSE</i>					
9		1.420 (1.436)	1.421	1.420	1.419
10		1.225 (1.213)	1.225	1.225	1.225
11		1.846 (1.837)	1.844	1.850	1.856



slightly shortens from 1.457 Å (**1**) to 1.451 Å (**2**). The B3LYP/6-31G** bond lengths calculated for **2** are in good agreement with the experimental solid-state X-ray data with differences in all cases within 0.015 Å. The introduction of end-capping dioxolane groups affects the outermost benzene rings and produce a lengthening of the single C–C bonds 3 and 4 and a shortening of the double C=C bond 2. Single bond 1 experiences a sizeable shortening due to the ring tension imposed by the attachment of the dioxolane ring. In contrast to the dioxolane groups, the electron-withdrawing chlorine atoms and cyano groups induce a significant lengthening of bond 1 from 1.432 Å in **2** to 1.441 and 1.453 Å in **4** and **5**, respectively, as well as a slight lengthening and shortening of adjacent double and single CC bonds (2 and 3, respectively). The bond length alternation between single and double bonds along the peripheral oligoenic ribbons therefore increases when electron-releasing dioxolane groups are incorporated and diminishes in passing from **2** to **4** and **5** due to the presence of electron-withdrawing groups.

3.2 Raman vibrational analysis

From the earliest studies on electrically conducting polymers, IR and Raman vibrational spectroscopies have been widely used to characterize many different types of π -conjugated systems, both oligomers and polymers, and

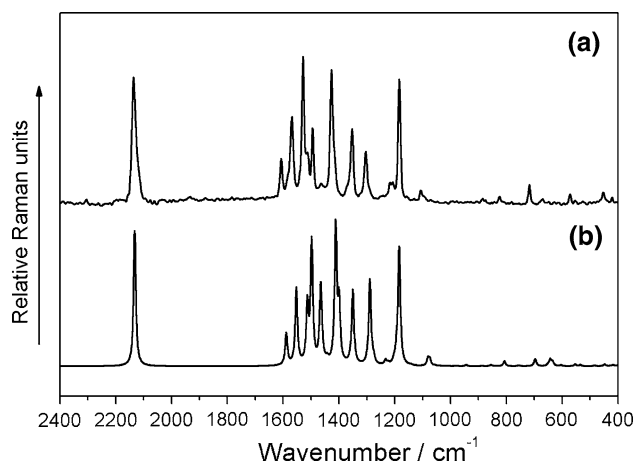


Fig. 2 Raman spectrum of derivative **4** over probe energies of 2,400–400 cm⁻¹. **a** Experimentally recorded in solid state. **b** Theoretically calculated at the B3LYP/6-31G** level. The intensity of the most intense theoretical band at 2,133 cm⁻¹ has been scaled by a factor of 0.2

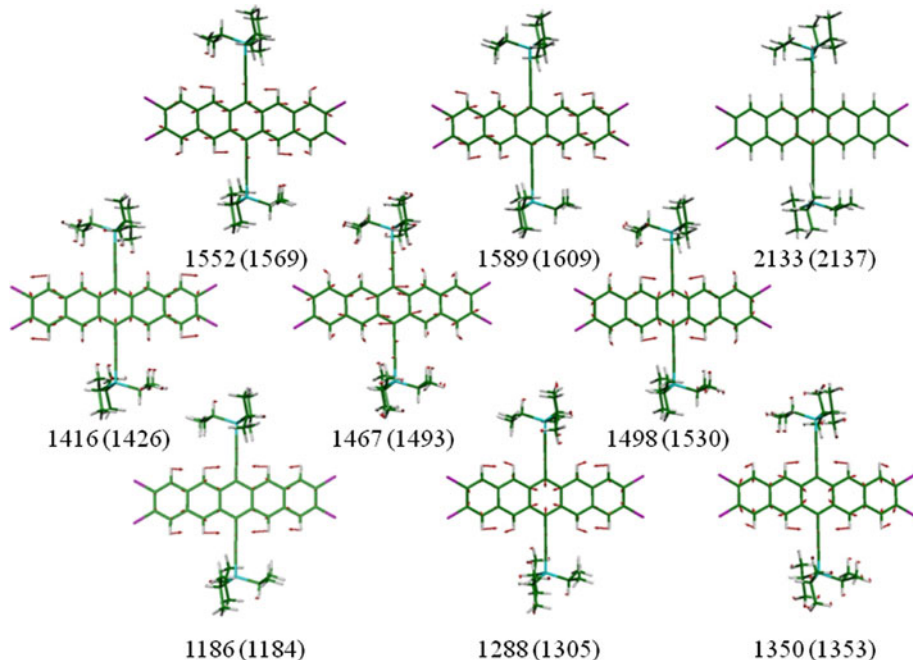
among them Raman spectroscopy has been shown to be of great help in (i) analyzing the effectiveness of the π -conjugation along a homologous series of oligomers [56–65], (ii) characterizing different types of conjugational defects induced by either chemical doping or photoexcitation [61, 66–70] and (iii) estimating the degree of intramolecular charge transfer in push–pull π -conjugated chromophores [12, 71–73]. Recent Raman studies focused on different homologous series of thiophene- and selenophene-based heteroacenes [74–77]. Despite the increasing attention on acene derivatives for applications in organic electronics,

there exists only a relatively small amount of Raman scattering information on these compounds.

Compound **4** has been selected as a representative example to analyze in detail the Raman spectrum of these functionalized pentacenes. Figure 2 displays the Raman spectrum recorded for compound **4** in the 2,400–400 cm⁻¹ energy region together with the theoretical B3LYP/6-31G** simulated spectrum. Figure 3 sketches the eigenvectors associated with the most outstanding Raman features of compound **4**, whereas Fig. 4 compares the B3LYP/6-31G** Raman spectra for pentacenes **1–5**.

The Raman spectrum of compound **4** presents many intense vibrational features of similar intensities in the 1,200–1,600 cm⁻¹ range, with the most intense peaks observed at 1,184, 1,426 and 1,530 cm⁻¹, and an isolated intense band at 2,137 cm⁻¹. The B3LYP/6-31G** Raman spectrum very nicely resembles the experimental one, both in peak position and relative intensities. The Raman band at 1,184 cm⁻¹ is calculated at 1,186 cm⁻¹ and corresponds to a totally symmetric in-plane C–H bond deformation coupled with a weak C–C/C=C stretching vibration which spreads over the whole pentacene spine (see Fig. 3). The experimental features at 1,426 and 1,530 cm⁻¹ are to be correlated with the theoretical vibrational modes computed at 1,416 and 1,498 cm⁻¹, respectively. These modes arise from C–C/C=C stretching vibrations on the whole pentacene backbone coupled with in-plane C–H bond deformations, the former being mainly located on the outermost rings and the latter on the innermost rings. In addition to these three intense features, the spectrum presents five medium-intensity peaks at 1,305, 1,353, 1,493, 1,569 and

Fig. 3 B3LYP/6-31G** eigenvectors calculated for selected Raman bands of **4**. Theoretical and experimental (within parentheses) wavenumbers are given in cm⁻¹



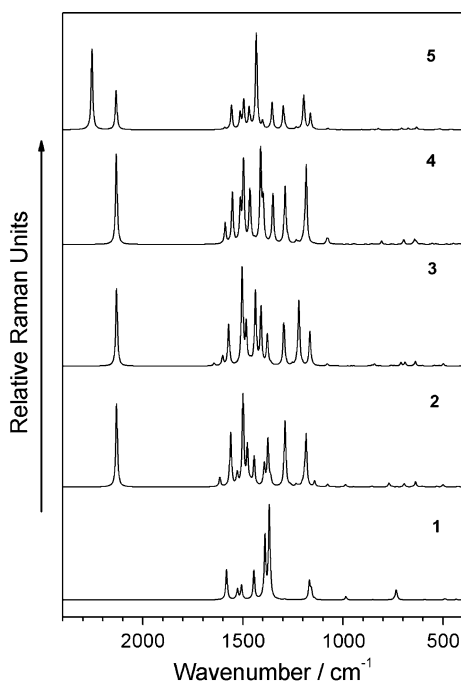


Fig. 4 B3LYP/6-31G** Raman profiles calculated for pentacenes **1–5**

1,609 cm^{-1} that are well predicted by B3LYP/6-31G** calculations at 1,288, 1,350, 1,467, 1,552 and 1,589 cm^{-1} , respectively (see Fig. 2). As sketched in Fig. 3, all these peaks also result from a combination of C–C/C=C stretching vibrations and in-plane C–H bendings. The highest energy modes at 1,552 and 1,589 cm^{-1} mainly imply a collective C–C/C=C movement of the peripheral oligoenic ribbons. Finally, the band at 2,137 cm^{-1} is to be assigned to the vibrational mode calculated at 2,133 cm^{-1} and is due to the totally symmetric stretching of the two ethynyl groups.

The comparative analysis of the Raman spectra computed for **1–5** shows that the attachment of the TIPSE groups to the central benzene ring gives rise to a significantly more complex spectral profile compared to unsubstituted pentacene. For compound **2**, two new intense features directly related to the TIPSE groups are computed to appear at 1,287 and 2,130 cm^{-1} , which are to be correlated with those experimentally measured at 1,304 and 2,125 cm^{-1} , respectively. The former is mainly associated with an in-plane C–H bending coupled to the breathing mode of the central benzene ring and corresponds to the vibrational mode computed at 1,288 cm^{-1} for **4** (see Fig. 3). The latter is due to the totally symmetric stretching of the two ethynyl groups and appears at very similar frequencies for compounds **2–5**. The relative intensities of the respective vibrational features of **1** and **2** are also altered upon the attachment of the TIPSE groups. For instance, the most intense band in the 1,200–1,600 cm^{-1}

region appears at 1,500 cm^{-1} for **2**. This band corresponds to that calculated at 1,498 cm^{-1} for **4** and mainly implies the vibration of the central benzene ring to which the TIPSE groups are attached (Fig. 3).

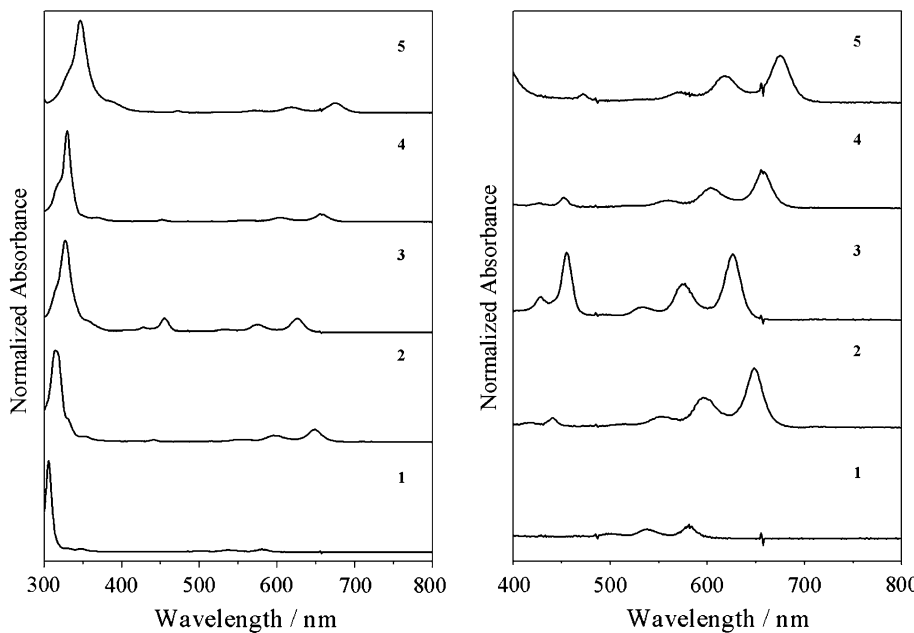
The Raman spectra of compounds **3**, **4** and **5** are quite similar to that computed for **2**. As expected, compound **5** presents an additional peak at 2,260 cm^{-1} , due the totally symmetric stretching of the C≡N bonds, that is observed at 2,234 cm^{-1} in the experimental spectrum. The unusual complexity of the Raman spectra obtained for **2–5** (i.e., many vibrational features with similar intensities and spreading over the whole spectral range) hinders an easy rationalization of the effects of the substituents on the vibrational properties.

3.3 Electronic absorption spectra

Figure 5 displays the normalized UV–Vis absorption spectra of **1–5** recorded in 1,2-dichlorobenzene. The electronic absorption spectra can be divided into three different wavelength regions. At high wavelengths (535–675 nm), pentacene derivatives **1–5** display a series of well-separated weak absorptions, which are assigned to the vibronic fine structure of the first electronic transition [78]. This vibronic structure results from the inherent molecular rigidity of the π -conjugated backbone of the pentacene moiety. Around 440 nm, it is possible to distinguish another two weaker absorptions, which appear somewhat intensified in the case of compound **3** (see Fig. 5, right). A third strong and structured absorption dominates the UV spectral region below 360 nm for pentacenes **1–5**. As can be seen in Fig. 5, the attachment of the different substituents gives rise to changes in the positions and relative intensities of the different absorption bands. The strongest band undergoes a remarkable red-shift due to the attachment of both the electron-releasing dioxolane groups (**3**) and the electron-withdrawing chlorine atoms (**4**) and cyano groups (**5**) to the end rings of the fused pentacene backbone. In contrast, the absorption band recorded at the longest wavelengths undergoes different shifts depending upon the substitution pattern. The dioxolane groups induce an appreciable blue-shift while electron-withdrawing chlorine atoms and cyano groups give rise to a slight red-shift.

To provide insight into the nature of the UV–Vis absorptions experimentally observed for **1–5** as well as their dependence on the substitution pattern, the singlet excited electronic states of all these pentacenes were calculated at the B3LYP/6-31G** level using the TDDFT approach and the previously optimized ground-state molecular geometries. Experimental and computed vertical excitation energies, oscillator strengths and the description of the electronic transitions in terms of the dominant one-

Fig. 5 Normalized UV–Vis–NIR absorption spectra of pentacenes **1–5** in 1,2-dichlorobenzene. *Left* Whole spectra in the 300–800 nm range. *Right* The spectral range is reduced to 400–800 nm to better visualize the less intense absorption bands



electron excitations are listed in Table 2. Figure 6 depicts the B3LYP/6-31G** energies and the topologies of the MOs mainly involved in the electronic transitions observed

in the absorption UV–Vis spectrum for **2**. Figure 6 is used as a guide to the TDDFT description of the excited states.

TDDFT calculations predict the existence of a few electronic transitions in the near-UV–visible range, which

Table 2 UV–Vis absorption maxima observed at room temperature and TDDFT//B3LYP/6-31G** vertical one-electron excitations calculated for **1–5**

Compound	Exp. (nm) ^a	Exp. (eV) ^a	TDDFT (eV) ^b	Description ^{c,d}
1	581 (537, 500)	2.13	1.94 (0.042)	H → L(0.62)
	348	3.56	3.25 (0.013)	H – 2 → L(0.54); H → L + 2(0.48)
	306	4.05	4.33 (3.229)	H – 2 → L(–0.39); H → L + 2(0.46)
2	648 (596, 552)	1.91	1.69 (0.177)	H → L(0.60)
	441	2.81	3.10 (0.071)	H – 2 → L(0.63); H → L + 2(0.29)
	351	3.53	3.56 (0.294)	H – 2 → L(0.25); H → L + 3(0.61)
	316	3.92	4.12 (2.137)	H – 3 → L(0.36); H → L + 3(0.50)
3	626 (575, 531)	1.98	1.79 (0.181)	H → L(0.61)
	454	2.73	2.87 (0.338)	H – 1 → L(0.62); H → L + 3(0.32)
	427	2.90	3.21 (0.069)	H – 3 → L(0.61); H → L + 2(0.33)
	357	3.47	3.59 (0.308)	H – 3 → L(0.29); H → L + 2(0.59)
	330	3.76	3.95 (1.774)	H – 1 → L(0.23); H → L + 3(0.58)
4	657 (603, 558)	1.89	1.66 (0.160)	H → L(0.60)
	453	2.74	3.00 (0.101)	H – 3 → L(0.58); H → L + 3(0.41)
			3.00 (0.067)	H – 2 → L(0.65); H → L + 2(0.25)
	368	3.37	3.50 (0.297)	H – 2 → L(0.21); H → L + 2(0.62)
5	330	3.76	3.86 (2.269)	H – 3 → L(0.33); H → L + 3(0.51)
	317	3.91	3.87 (0.133)	H – 8 → L(0.67)
	675 (618, 571)	1.84	1.60 (0.142)	H → L(0.60)
5	473	2.62	2.81 (0.039)	H – 6 → L(0.44); H → L + 2(0.56)
			2.88 (0.056)	H – 2 → L(0.67); H → L + 3(0.19)
	384	3.23	3.39 (0.230)	H – 7 → L(0.40); H → L + 3(0.54)
	347	3.57	3.56 (2.473)	H – 6 → L(0.50); H → L + 2(–0.37)
	332	3.73	3.59 (0.149)	H – 7 → L(0.56); H → L + 3(0.36)

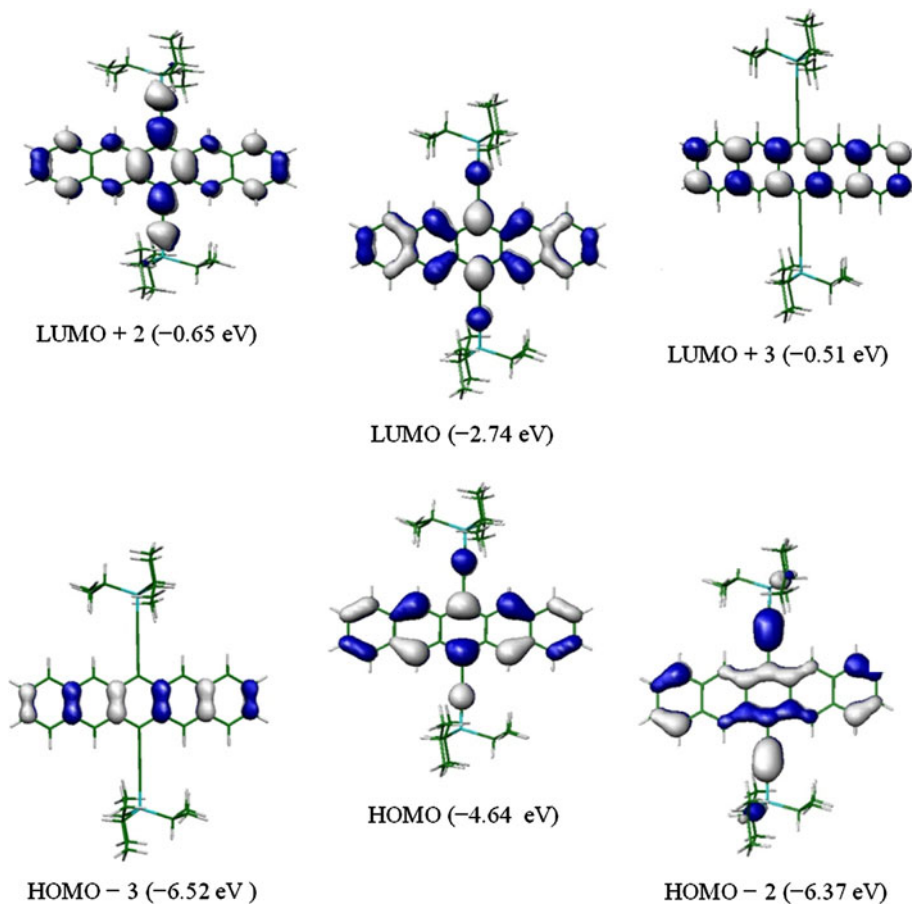
^a Absorption maxima (in nm and eV) from the experimental spectra displayed in Fig. 5; values within parentheses correspond to vibronic peaks

^b B3LYP/6-31G** vertical excitation energies (in eV) and oscillator strengths (*f*) within parentheses

^c HOMO and LUMO are abbreviated as H and L, respectively

^d The weight of one-electronic excitations is given within parentheses

Fig. 6 B3LYP/6-31G** electronic density contours (0.03 e bohr^{-3}) and energies calculated for selected MOs of the pentacene derivative **2**



also deserve to be analyzed separately into three different regions, as previously performed for the experimental absorption bands. All the electronic transitions quoted in Table 2 for compounds **2–5** imply $\pi-\pi^*$ excitations to ${}^1\text{B}_u$ states and are polarized in the molecular plane thus bearing the largest intensities. The lowest-energy transition computed at 1.94 eV (oscillator strength $f = 0.042$) for **1**, 1.69 eV ($f = 0.177$) for **2**, 1.79 eV ($f = 0.181$) for **3**, 1.66 eV ($f = 0.160$) for **4** and 1.60 eV ($f = 0.142$) for **5** corresponds to the excitation to the first singlet excited state ($\text{S}_0 \rightarrow \text{S}_1$) and mainly implies a one-electron promotion from the HOMO to the LUMO. These molecular orbitals are delocalized on the conjugated CC skeleton (see Fig. 6). Since no other electronic transition is calculated below 2.6 eV, the three-peak structured band measured experimentally in the 580–675 nm (2.13–1.84 eV) range is, therefore, assigned to the $\text{S}_0 \rightarrow \text{S}_1$ electronic transition. The calculated excitation energies are in good agreement with the experimental values within 0.2 eV for all the pentacene derivatives **1–5**. The calculated $\text{S}_0 \rightarrow \text{S}_1$ transition undergoes a remarkable red-shift of 0.25 eV upon the attachment of the TIPSE groups. This shift results from the stabilization of the LUMO in passing from **1**

(−2.40 eV) to **2** (−2.74 eV) due to the elongation of bonds number 8 of the central benzene ring (0.023 Å, see Table 1), which diminishes the antibonding interactions that take place in the LUMO (see Fig. 6). Electron-withdrawing groups produce an additional red-shift of the computed $\text{S}_0 \rightarrow \text{S}_1$ transition in compounds **4** and **5** in agreement with the experimental observations. In contrast, dioxolane groups induce a blue-shift compared to derivative **2**. This shift is due to the structural changes induced on the outermost benzene rings by the attachment of the dioxolane groups that destabilize in a higher degree the LUMO level and increase the HOMO–LUMO gap in passing from **2** (1.90 eV) to **3** (2.02 eV). Therefore, TDDFT calculations explain the trends experimentally observed for the lowest-energy absorption band with the substitution pattern.

In increasing order of energy, the two following allowed electronic transitions are predicted at intermediate energies (2.81–3.25 eV) and are in general weaker ($f < 0.10$) than the $\text{S}_0 \rightarrow \text{S}_1$ excitation (see Table 2). These transitions correspond to $\text{S}_0 \rightarrow \text{S}_3$ and $\text{S}_0 \rightarrow \text{S}_4$ excitations for derivatives **1–4** ($\text{S}_0 \rightarrow \text{S}_3$ and $\text{S}_0 \rightarrow \text{S}_5$ for **5**) and, for compound **2**, are mainly described by the HOMO – 2, HOMO –

$3 \rightarrow$ LUMO excitations with a smaller contribution from the HOMO \rightarrow LUMO + 2, LUMO + 3 promotions (see Table 2; Fig. 6). It is to be noted that, although the substitution pattern alters the energy ordering of the MOs, the MOs involved in those transitions for compounds **3–5** indeed display the same topology than those participating in **2**. These transitions are to be correlated with those experimentally recorded in the 473- to 427-nm (2.62–2.90 eV) spectral range, whose relative intensity is rather weak except for **3**. The intensification of this band is also supported by TDDFT calculations that predict the $S_0 \rightarrow S_3$ excitation of **3** with a larger oscillator strength ($f = 0.308$) than for the remaining pentacene derivatives. Compared to unsubstituted pentacene **1**, all the absorption features observed in the visible increase their intensity upon functionalization (see Fig. 5; Table 2).

In the UV spectral range, TDDFT calculations also predict the appearance of a few strong electronic absorptions in full agreement with the experimental measurements. The first optical transition in this region is computed within the 3.39–3.59 eV energy range with a moderate oscillator strength ($f \sim 0.300$), and mainly arises from the HOMO \rightarrow LUMO + 2 one-electron excitation (HOMO \rightarrow LUMO + 3 for **5**). The weak UV absorption recorded at 351 nm (3.53 eV) for compound **2** is, therefore, assigned to the $S_0 \rightarrow S_8$ excitation computed at 3.56 eV. For the remaining pentacenes **3–5**, the corresponding weak absorption is partially masked by the quite close strongest absorption band and appears at progressively decreasing energies (3.47, 3.37 and 3.23 eV, respectively) in agreement with theoretical predictions (3.59, 3.50 and 3.39 eV, respectively).

Finally, the strongest electronic transition is predicted at 4.33 eV ($f = 3.229$) for **1**, 4.12 eV ($f = 2.137$) for **2**, 3.95 eV ($f = 1.774$) for **3**, 3.86 eV ($f = 2.269$) for **4** and 3.56 eV ($f = 2.473$) for **5**. It corresponds to the $S_0 \rightarrow S_6$ (**1**), $S_0 \rightarrow S_{10}$ (**3**) and $S_0 \rightarrow S_{11}$ (**2**, **4** and **5**) excitations and is described by the same one-electron promotions implied in the transitions calculated at intermediate energies (2.81–3.25 eV) but with a larger contribution from the HOMO \rightarrow LUMO + 2, LUMO + 3 promotions (see Table 2). This excitation is to be unambiguously assigned to the strongest UV optical absorption measured in the 300–350-nm range. TDDFT calculations nicely account for the sizeable red-shift of this absorption band as different substituents are attached to the terminal fused benzene rings. For derivatives **4** and **5**, another optical absorption is computed at 3.87 and 3.59 eV, with oscillator strengths of 0.133 and 0.149, respectively, that matches quite well with the shoulders experimentally measured at 317 and 332 nm (3.91 and 3.73 eV) for **4** and **5**, respectively. Thus, TDDFT calculations have enabled for a satisfactory description and quantitative assignment of the UV–Vis absorption spectra of the pentacene derivatives **1–5**.

4 Conclusions

This work presents an analysis of the evolution of the molecular, vibrational and optical properties with the substitution pattern of a family of functionalized pentacenes (**1–5**). The analysis is performed by quantum-chemical calculations based on the density functional theory (DFT and TDDFT) approach in combination with spectroscopic techniques (Raman and UV–Vis).

Pentacenes **1–5** can be visualized as two parallel oligoenic ribbons linked by single C–C bonds. The bond length alternation between single and double C–C/C=C bonds along each oligoenic ribbon progressively diminishes on going from the outer to the central rings indicating an efficient electron delocalization along the periphery of the π -conjugated backbone. The attachment of TIPSE groups mainly affects the central benzene ring to which they are attached. The bond length alternation between single and double bonds along the peripheral oligoenic ribbons increases when electron-releasing dioxolane groups are incorporated and diminishes when electron-withdrawing chlorine atoms and cyano groups are introduced.

The functionalized pentacenes (**2–5**) display Raman spectra with many intense features of similar intensities in the 1,200–1,600 cm^{-1} range. The complexity of the Raman spectrum increases with the attachment of the triisopropylsilyl ethynyl groups and makes difficult the rationalization of the effect of the substitution pattern on the vibrational properties. The strongest Raman features mainly correspond to a combination of C–C/C=C stretching vibrations and in-plane C–H deformations which spread over the whole pentacene backbone.

TDDFT calculations enable a satisfactory description and the assignment of the UV–Vis absorption spectra of pentacenes **1–5**. The spectra imply $\pi\text{-}\pi^*$ excitations to ${}^1\text{B}_\text{u}$ states that are polarized in the molecular plane. The experimentally three-peak band observed at low energies (2.13–1.84 eV) is assigned to the HOMO \rightarrow LUMO $S_0 \rightarrow S_1$ electronic transition. Theoretical calculations account for the red-shift caused by the attachment of the TIPSE groups. They also predict the blue-shift induced by the dioxolane groups and the additional red-shift produced by the electron-withdrawing chlorine atoms and cyano groups. The shifts result from the stabilization/destabilization of the LUMO in passing from **1–5**. At intermediate energies (2.81–3.25 eV), weak electronic transitions are calculated for **2–5** that appear to be intensified for **3** in agreement with experimental data. The strongest electronic transitions are predicted in the 4.33–3.56 eV range in good correlation with the strongest UV bands observed at 4.13–3.54 eV. These excitations undergo a sizeable red-

shift, which is well-reproduced by TDDFT calculations, as substituents are attached to the terminal benzene rings.

Acknowledgments This work was supported by the Ministerio de Ciencia e Innovación (MICINN) of Spain (projects CTQ2009-08790, CTQ2009-10098 and Consolider-Ingenio CSD2007-00010 in Molecular Nanoscience). The authors are also indebted to Junta de Andalucía for the project of excellence P09-FQM-4708 and grant FQM-159. The MICINN and UMA are also gratefully acknowledged by J.A. and R.M.O. for a FPI doctoral grant and a research grant, respectively.

References

- Anthony JE (2006) *Chem Rev* 106:5028
- Anthony JE (2008) *Angew Chem Int Ed* 47:452
- Podzorov V, Menard E, Borissov A, Kiryukhin V, Rogers JA, Gershenson ME (2004) *Phys Rev Lett* 93:086602
- Brédas J-L, Calbert JP, Da Silva Filho DA, Cornil J (2002) *Proc Natl Acad Sci USA* 99:5804
- Gundlach DJ, Lin YY, Jackson TN, Nelson SF, Schlom DG (1997) *IEEE Electron Device Lett* 18:87
- Anthony JE, Brooks JS, Eaton DL, Parkin SR (2001) *J Am Chem Soc* 123:9482
- Anthony JE, Eaton DL, Parkin SR (2002) *Org Lett* 4:15
- Maliakal A, Raghavachari K, Katz H, Chandross E, Siegrist T (2004) *Chem Mater* 16:4980
- Park SK, Jackson TN, Anthony JE, Mourey DA (2007) *Appl Phys Lett* 91:063514
- Paine MM, Delcamp JH, Parkin SR, Anthony JE (2004) *Org Lett* 6:1609
- Swartz CR, Parkin SR, Bullock JE, Anthony JE, Mayer AC, Malliaras GG (2005) *Org Lett* 7:3163
- Casado J, Pappfenbus TM, Miller LL, Mann KR, Ortí E, Viruela PM, Pou-Amérigo R, Hernández V, López Navarrete JT (2003) *J Am Chem Soc* 125:2524
- Ortí E, Viruela PM, Effenberger F, Hernández V, López Navarrete JT (2005) *J Phys Chem A* 109:8724
- Casado J, Zgierski MZ, Hicks RG, Myles DJT, Viruela PM, Ortí E, Ruiz Delgado MC, Hernández V, López Navarrete JT (2005) *J Phys Chem A* 109:11275
- Ponce Ortiz R, Casado J, Hernández V, López Navarrete JT, Ortí E, Viruela PM, Milián B, Hotta S, Zotti G, Zecchin S, Vercelli B (2006) *Adv Funct Mater* 16:531
- Ponce Ortiz R, Casado J, Rodríguez S, Hernández V, López Navarrete JT, Viruela PM, Ortí E, Takimiya K, Otsubo T (2010) *Chem Eur J* 16:470
- Ponce Ortiz R, Casado J, Hernández V, López Navarrete JT, Viruela PM, Ortí E, Takimiya K, Otsubo T (2007) *Angew Chem Int Ed* 46:9057
- Zade SS, Bendikov M (2007) *Chem Eur J* 13:3688
- Rubio M, Merchán M, Ortí E, Roos B (1995) *J Chem Phys* 102:3580
- Rubio M, Merchán M, Ortí E, Roos B (1996) *Chem Phys Lett* 248:321
- Rubio M, Ortí E, Pou-Amérigo R, Merchán M (2001) *J Phys Chem A* 105:9788
- Rubio M, Merchán M, Pou-Amérigo R, Ortí E (2003) *Chem Phys Chem* 4:1308
- Rubio M, Merchán M, Ortí E (2005) *Chem Phys Chem* 6:1357
- Zade SS, Bendikov M (2006) *J Phys Chem B* 110:15839
- Zamoshchik N, Salzner U, Bendikov M (2008) *J Phys Chem C* 112:8408
- Aragó J, Viruela PM, Ortí E (2009) *J Mol Struct (Theochem)* 912:27
- Cuesta IG, Aragó J, Ortí E, Lazzeretti P (2009) *J Chem Theory Comput* 5:1767
- Aragó J, viruela PM, Ortí E, Osuna RM, Vercelli B, Zotti G, Hernández V, López Navarrete JT, Henssler JT, Matzger AJ, Suzuki Y, Yamaguchi S (2010) *Chem Eur J* 16:5481
- Frisch MJ, Trucks GW, Schlegel HB, Scuseria GE, Robb MA, Cheeseman JR, Montgomery JA, Vreven JT, Kudin KN, Burant JC, Millam JM, Iyengar SS, Tomasi J, Barone V, Mennucci B, Cossi M, Scalmani G, Rega N, Petersson GA, Nakatsuji H, Hada M, Ehara M, Toyota K, Fukuda R, Hasegawa J, Ishida M, Nakajima T, Honda Y, Kitao O, Nakai H, Klene M, Li X, Knox JE, Hratchian HP, Cross JB, Adamo C, Jaramillo J, Gomperts R, Stratmann RE, Yazyev O, Austin AJ, Cammi R, Pomelli C, Ochterski JW, Ayala PY, Morokuma K, Voth GA, Salvador P, Dannenberg JJ, Zakrzewski VG, Dapprich S, Daniels AD, Strain MC, Farkas O, Malick DK, Rabuck AD, Raghavachari K, Foresman JB, Ortiz JV, Cui Q, Baboul AG, Clifford S, Cioslowski J, Stefanov BB, Liu G, Liashenko A, Piskorz P, Komaromi I, Martin RL, Fox DJ, Keith T, Al-Laham MA, Peng CY, Nanayakkara A, Challacombe M, Gill WPM, Johnson B, Chen W, Wong MW, Gonzalez C, Pople JA (2004) Gaussian 03, revision D.02. Gaussian Inc., Wallingford CT
- Becke AD (1993) *J Chem Phys* 98:5648
- Lee C, Yang W, Parr RG (1988) *Phys Rev B* 37:785
- Franci MM, Pietro WJ, Hehre WJ, Binkley JS, Gordon MS, Defrees DJ, Pople JA (1985) *J Chem Phys* 77:3654
- Scott AP, Radom L (1996) *J Phys Chem* 100:16502
- Rauhut G, Pulay P (1995) *J Phys Chem* 99:3093
- Jiménez-Hoyos CA, Janesko BJ, Scuseria GE (2008) *Phys Chem Chem Phys* 10:6621
- Casida ME, Jamorski C, Casida KC, Salahub DR (1998) *J Chem Phys* 108:4439
- Jamorski C, Casida ME, Salahub DR (1996) *J Chem Phys* 104:5134
- Petersilka M, Grossmann UJ, Gross EKU (1996) *Phys Rev Lett* 76:1212
- Hsu CP, Hirata S, Head-Gordon M (2001) *J Phys Chem A* 105:451
- Parac M, Grimme S (2003) *Chem Phys* 292:11
- Weisman JL, Lee TJ, Head-Gordon M (2001) *Spectrochim Acta A* 57:931
- Hirata S, Lee TJ, Head-Gordon M (1999) *J Chem Phys* 111:8904
- Heinze HH, Görling A, Rösch N (2000) *J Chem Phys* 113:2088
- Hirata S, Head-Gordon M, Szcsepanski J, Vala M (2003) *J Chem Phys* 107:4940
- Halasinski TM, Weisman JL, Ruiterkamp R, Lee TJ, Salama F, Head-Gordon M (2003) *J Phys Chem A* 107:3660
- Bauerndschmitt R, Ahlrichs R, Heinrich FH, Kappes MM (1998) *J Am Chem Soc* 120:5052
- Pogantsch A, Heimel G, Zojer E (2002) *J Chem Phys* 117:5921
- Hutchinson GR, Ratner MA, Marks RN (2002) *J Phys Chem A* 106:10596
- van Gisbergen SJA, Rosa A, Ricciardi G, Baerends EJ (1999) *J Chem Phys* 114:10757
- Nguyen KA, Pachter R (2001) *J Chem Phys* 114:10757
- Jaworska M, Kazibut G, Lodziński P (2003) *J Phys Chem A* 107:1339
- Yamaguchi Y (2002) *J Chem Phys* 117:9668
- Pou-Amérigo R, Viruela PM, Viruela R, Rubio M, Ortí E (2002) *Chem Phys Lett* 352:491
- Portmann S, Lüthi HP (2000) *Chimia* 54:766
- Bendikov M, Duong HM, Starkey K, Houk KN, Carter EA, Wudl F (2004) *J Am Chem Soc* 126:7416

56. Ruiz Delgado MC, Hernández V, López Navarrete JT, Tanaka S, Yamashita Y (2004) *J Phys Chem B* 108:2516
57. Sakamoto A, Furukawa Y, Tasumi M (1994) *J Phys Chem* 98:4635
58. Yokonuma N, Furukawa Y, Tasumi M, Kuroda M, Nakayama J (1996) *Chem Phys Lett* 255:431
59. Harada I, Furukawa Y (1991) Vibrational spectra and structure. Elsevier, Amsterdam, The Netherlands
60. Hernández V, Casado J, Ramirez FJ, Zotti G, Hotta S, López Navarrete JT (1996) *J Chem Phys* 104:9271
61. Casado J, Hernández V, Hotta S, López Navarrete JT (1998) *J Chem Phys* 109:10419
62. Moreno Castro C, Ruiz Delgado MC, Hernández V, Hotta S, Casado J, López Navarrete JT (2002) *J Chem Phys* 116:10419
63. Moreno Castro C, Ruiz Delgado MC, Hernández V, Shirota Y, Casado J, López Navarrete JT (2002) *J Phys Chem B* 106:7163
64. Ruiz Delgado MC, Casado J, Hernández V, López Navarrete JT, Fuhrmann G, Bauerle P (2004) *J Phys Chem B* 108:3158
65. Casado J, Ponce Ortiz R, Ruiz Delgado MC, Azumi R, Oakley RT, Hernández V, López Navarrete JT (2005) *J Phys Chem B* 109:10115
66. Casado J, Hernández V, Hotta S, López Navarrete JT (1998) *Adv Mater* 10:1258
67. Casado J, Miller LL, Mann KR, Pappendorf TM, Kanemitsu Y, Ortí E, Viruela PM, Pou-Amérigo R, Hernández V, López Navarrete JT (2002) *J Phys Chem B* 106:3872
68. Casado J, Miller LL, Mann KR, Pappendorf TM, Hernández V, López Navarrete JT (2002) *J Phys Chem B* 106:3597
69. Casado J, Ruiz Delgado MC, Shirota Y, Hernández V, López Navarrete JT (2003) *J Phys Chem B* 107:2637
70. Casado J, Hernández V, Ponce Ortiz R, Ruiz Delgado MC, López Navarrete JT, Fuhrmann G, Bauerle P (2004) *J Raman Spectrosc* 35:592
71. Hernández V, Casado J, Effenberger F, López Navarrete JT (2000) *J Chem Phys* 112:5105
72. Casado J, Hernández V, Kim OK, Lehn JM, López Navarrete JT, Delgado Ledesma S, Ponce Ortiz R, Ruiz Delgado MC, Vida Y, Perez-Inestrosa E (2004) *Chem Eur J* 10:3805
73. González M, Segura JL, Seoane C, Martín N, Garín J, Orduna J, Alcalá R, Villacampa B, Hernández V, López Navarrete JT (2001) *J Org Chem* 66:8872
74. Malavé Osuna R, Zhang X, Matzger AJ, Hernández V, López Navarrete JT (2006) *J Phys Chem A* 110:5058
75. Malavé Osuna R, Ponce Ortiz R, Okamoto T, Suzuki Y, Yamaguchi S, Hernández V, López Navarrete JT (2007) *J Chem Phys* B 111:7488
76. Malavé Osuna R, Ponce Ortiz R, Ruiz Delgado MC, Nenajdenko VG, Sumerin VV, Balenková ES, Hernández V, López Navarrete JT (2007) *ChemPhysChem* 8:745
77. Malavé Osuna R, Hernández V, López Navarrete JT, Aragó J, Viruela PM, Ortí E, Suzuki T, Yamaguchi S, Henssler JT, Matzger AJ (2009) *ChemPhysChem* 10:3069
78. Halasinski TM, Hudgins DM, Salama F, Allamandola LJ, Bally T (2000) *J Phys Chem A* 104:7484